https://doi.org/10.20965/ijat.2013.p0016

Paper:

Simulation of Microstructure Evolution and Deformation Behavior for Dual-Phase Steel by Multi-Phase-Field Method and Elastoplastic Finite Element Method

Akinori Yamanaka* **and Tomohiro Takaki****

*Graduate School of Engineering, Tokyo University of Agriculture and Technology
2-24-16 Nakacho, Koganei, Tokyo 184-8588, Japan
E-mail: a-yamana@cc.tuat.ac.jp
**Graduate School of Science and Technology, Kyoto Institute of Technology
Goshokaidoucho, Matsugasaki, Sakyo, Kyoto 606-8585, Japan
E-mail: takaki@kit.ac.jp
[Received August 11, 2012; accepted November 29, 2012]

A coupled simulation method is developed by using a Multi-Phase-Field (MPF) method that is recognized as a powerful numerical method for simulating microstructure formation in material and ElastoPlastic Finite Element Analysis (EP-FEA) based on a homogenization method. We apply the developed simulation method to investigate the deformation behavior of DP steel that includes various volume fractions and morphologies of the ferrite (α) phase. To obtain morphological information on the α phase of DP steel, we performed MPF simulation of austenite-to-ferrite ($\gamma \rightarrow \alpha$) transformation during continuous cooling transformation. MPF simulation gives us the digital image of the distribution of the simulated α phase. Furthermore, we model the representative volume element, which describes the DP microstructure, on the basis of the obtained morphology of the α phase, and perform tension-compression testing of DP steel, including the simulated α phase. Through these simulations, it is confirmed that the developed simulation method enables us to clarify the effect of the volume fraction and the configuration of the α phase on macroscopic deformation behavior of DP steel, such as the Bauschinger effect.

Keywords: multi-phase-field method, elastoplastic finite element method, homogenization method, dual-phase steel, phase transformation

1. Introduction

The mechanical properties of steels are strongly affected by their underlying microstructure. Specifically, the deformation behavior of Dual-Phase (DP) steel, which possesses high strengh, toughness and good formability, is characterized by the volume fraction and distribution of soft ferrite (α) and hard martensite (α') phases [1]. In order to improve the mechanical properties of DP steel, it is therefore essential to understand the relationship between the microstructure and deformation behavior. However, it is difficult to predict various microstructure evolutions occured in steel making processes and the mechanical properties of DP steel only by experiments.

In the past few decades, considerable efforts have been made to predict microstructure evolution and mechanical properties of steels using numerical approaches [2, 3]. Recently, the Phase-Field Method (PFM) has been recognized as an innovative numerical approach for simulating various microstructure evolutions in materials [4]. More recently, the Multi-Phase-Field Method (MPFM) has proposed to simulate microstructure evolutions in polycrystalline multiphase materials [5, 6]. The PFM and MPFM have been used to simulate various microstructure evolutions during solidification [7, 8], phase transformation [9, 10], recrystallization [11, 12]. Although the Cellular Automaton (CA) and the Monte-Carlo (MC) methods have been also used to simulate many microstructure evolutions in materials, these methods have limitations, as the CA method cannot describe curvature-driven interface migration and the MC method cannnot account correctly for timescales, while the PFM and MPFM can solve the above problems. The most attractive advantage of the PFM and MPFM is that they enable us to simulate morphological change in a simulated microstructure on the basis of the total free energy of the material.

In comparison, a Finite Element Analysis (FEA) based on the mathematical homogenization method has been studied actively as a powerful numerical approach for investigating both macro- and microscopic deformation behavior of a material, including the heterogeneous microstructure [13, 14]. Terada et al. proposed two-scale FEA based on the homogenization method for a heterogeneous solid and used it in order to clarify the Bauschinger effect in carbon steel [15]. Therefore, a coupled numerical model using the MPFM and FEA based on the homogenization method is useful in systematically predicting the microstructure and the mechanical properties of steels.

In a previous study, the authors developed a numer-

ical simulation model by coupling PFM with EP-FEA based on the homogenization method [16]. The developed model was used to simulate the formation of microstructure during austenite-to-ferrite ($\gamma \rightarrow \alpha$) transformation in a Fe-C alloy. Furthermore, on the basis of the morphology of the simulated microstructure, we performed FEA of uniaxial tensile testing of α + pearlite steel, which contains the simulated α phase. Through these simulations, macroscopic stress-strain curves and distribution of microscopic plastic strain in the microstructure have been clarified. However, in the previous study, the evolution of the α phase was simulated only in a single austenite (γ) grain. In order to apply the coupled simulation model to practical steel development, it is essential to predict microstructure evolution and deformation behavior in polycrystalline multiphase steel.

In this paper, we propose a new coupled simulation method to predict microstructure evolution and the deformation behavior of polycrystalline multiphase steel by using the MPFM and EP-FEA based on the homogenization method. We use the proposed simulation method to investigate the deformation behavior of DP steel containing the α phase predicted by MPF simulation. This paper is organized as follows. In section 2, the MPF model of $\gamma \rightarrow \alpha$ transformation is explained. To simulate $\gamma \rightarrow \alpha$ transformation in a polycrystalline Fe-C-Mn alloy during Continuous Cooling Transformation (CCT), we derive two differential equations that are used for describing the motion of the α/γ interface and carbon diffusion during $\gamma \rightarrow \alpha$ transformation. In section 3, EP-FEA is explained based on the mathematical homogenization theory. In section 4, simulation models are explained for MPF simulation and EP-FEA. In section 5, results are explained for MPF simulation of the $\gamma \rightarrow \alpha$ transformation. Then, we explain EP-FEA of the tension-compression test of DP steel, including the simulated α phase. The effects of volume fraction and distribution of the α phase on the deformation behavior of the DP steel are investigated on the basis of results obtained from these simulations.

2. Multi-Phase-Field Method

In this study, $\gamma \rightarrow \alpha$ transformation in a Fe-C-Mn alloy during CCT is simulated by the generalized MPFM proposed by Steinbach et al. [17]. Using this MPF model, we describe multiple-junction points precisely by introducing an additional interface-field. Furthermore, since $\gamma \rightarrow \alpha$ transformation in steel accompanies the diffusion of carbon atoms between the α and γ phases, the carbon diffusion equation of the multi-phase system is solved. Although Eiken et al. [18] proposed an MPFM with the diffusion equation derived from total free energy, we employ the diffusion equation with the linearized phase diagram proposed by Tiaden et al. [19] for simplicity. We also assume that the para-equilibrium condition is satisfied during transformation and that the diffusion of Mn atoms is ignored.

We use N phase-field variables ϕ_i ($i = 1, 2, \ldots, N$) by considering a system of N crystal grains. ϕ_i describes the fraction of the i-th grain and varies smoothly across an interface from $\phi_i = 1$ in the i-th grain to $\phi_i = 0$ in another grain. Thus, all phase-field variables satisfy constraint $\sum_{i=1}^{N} \phi_i = 1$ at all points. Using phase-field variables, total Gibbs free energy of system G is defined as a Ginzburg–Landau-type Gibbs free energy functional that is given by the sum of a gradient energy that describes additional energy due to the existence of an interface, potential energy and bulk free energy as [17]:

$$G = \int_V \left\{ \sum_{i=1}^{N} \sum_{j=i+1}^{N} \left(-\frac{a_{ij}^2}{2} \nabla\phi_i \cdot \nabla\phi_j + W_{ij}\phi_i\phi_j \right) + g \right\} dV \quad \ldots \ldots (1)$$

where a_{ij}, W_{ij}, and g are gradient coefficient, potential height, and bulk free energy density, respectively. These parameters are related to interfacial energy between grains i and j, γ_{ij}, and interfacial thickness δ as $a_{ij} = 2\sqrt{2\delta\gamma_{ij}}/\pi$ and $W_{ij} = 4\gamma_{ij}/\delta$.

Assuming that the microstructure evolves so that total free energy decreases monotonically with time, the evolution equation of the phase-field variables is derived as

$$\frac{\partial \phi_i}{\partial t} = -\frac{2}{n} \sum_{j=1}^{n} M_{ij}^{\phi} \left[\sum_{k=1}^{n} \left\{ \left(W_{ik} - W_{jk} \right) \phi_k + \frac{1}{2} \left(a_{ik}^2 - a_{jk}^2 \right) \nabla^2 \phi_k - \frac{8}{\pi} \sqrt{\phi_i \phi_j} \Delta G_{ij} \right\} \right] \quad \ldots (2)$$

where n is the number of phase fields at an arbitrary point and is given by $n = \sum_{i=1}^{N} \xi_i$. Here, ξ_i is a step function that is expressed as $\xi_i = 1$ in region $0 < \phi_i \leq 1$ and as $\xi_i = 0$ elsewhere. The third term on the right side of Eq. (2) describes the phenomenological thermodynamic driving force of transformation. The magnitude of driving force ΔG_{ij} is given by $\Delta G_{\alpha\gamma} = \Delta S \Delta T$ at the α/γ interface, where ΔS and ΔT are the entropy difference between the α and γ phases and undercooling, respectively [20]. The mobility of phase field M_{ij}^{ϕ} is given by $M_{ij}^{\phi} = \pi^2 M / 8\delta$, which is set to be a nonzero value only at the α/γ interface. M is the mobility of the α/γ interface, expressed as $M = M_0 \exp(-Q_0/RT)$. In numerical simulation, the migration of an interface can be simulated by calculating Eq. (2) using a second-order finite difference scheme for space and a first-order forward Euler-type finite difference method for time on a regular two-dimensional computational grid.

To simulate the diffusion of carbon atoms during $\gamma \rightarrow \alpha$ transformation in a multiphase system, total carbon concentration C is defined as a linear function of local carbon concentration c_i weighted by corresponding phase-field variables ϕ_i. Local carbon concentration is given by $c_i = k_i C / \sum_{j=1}^{n} k_j \phi_j$. Here, k_i is the partition coefficient of carbon atoms and is defined as the ratio of the equilibrium carbon concentration in the i-th grain to that in the γ phase [19]. Now, we consider an $\alpha + \gamma$ two-grain system ($N = n = 2$) for simplicity. When ϕ_1 and ϕ_2 correspond to α and γ phases, respectively, total carbon concentration is

written as

$$C = \sum_{i=1}^{n} \phi_i c_i = \phi_1 c_1 + \phi_2 c_2 \quad \ldots\ldots\ldots (3)$$

Using Eq. (3), the diffusion equation for total carbon concentration can be expressed as the sum of the diffusion fluxes of carbon atoms in individual grains as

$$\frac{\partial C}{\partial t} = \nabla \cdot \left(\sum_{i=1}^{n} \phi_i D_i^C \nabla c_i \right) = \nabla \cdot \left(\phi_1 D_1^C \nabla c_1 + \phi_2 D_2^C \nabla c_2 \right) \quad \ldots\ldots\ldots\ldots\ldots\ldots (4)$$

Here, D_i^C denotes the diffusion coefficient of carbon atoms in the i-th grain. When ϕ_1 and ϕ_2 are the phase field variables for α and γ phases, D_1^C and D_2^C correspond to diffusion coefficients for carbon atoms in α and γ phases. Carbon diffusion coefficients in the γ and α phases are as follows:

$$D_\gamma^C = D_0^\gamma \exp\left(\frac{-Q_\gamma}{RT}\right) \quad \ldots\ldots\ldots (5)$$

$$D_\alpha^C = D_0^\alpha \exp\left(\frac{-Q_\alpha}{RT}\right) \quad \ldots\ldots\ldots (6)$$

where D_0^α, D_0^γ, Q_α, and Q_γ are the pre-exponential factor and the activation energy of the diffusion coefficient in α and γ phases. Partition coefficient k_i and undercooling ΔT are derived from a linearized phase diagram [20, 21]. In numerical simulation, governing equations are solved by the finite difference method.

3. Elastoplastic Finite Element Method Based on Homogenization Method

In order to investigate deformation behavior in the tension-compression test of DP steel, including the simulated microstructure on the micro- and macroscopic scales, large-deformation EP-FEA based on the homogenization method is performed in two dimensions. In this FEA, DP steel is assumed to be an isotropic elasto-plastic material, and its deformation behavior is characterized by J_2 flow theory. Therefore, we employ the following constitutive equation, which is described by the Jaumann rate of Kirchhoff stress tensor $\overset{\nabla}{S}_{ij}$ and strain rate tensor $\dot{\varepsilon}_{ij}$ for large deformation [22]:

$$\overset{\nabla}{S}_{ij} = \left\{ D_{ijkl}^e - \frac{3G}{\bar{\sigma}^2 \left(\frac{H'}{3G} + 1 \right)} \sigma'_{ij} \sigma'_{kl} \right\} \dot{\varepsilon}_{kl} \quad . \quad (7)$$

where D_{ijkl}^e, σ'_{ij}, $\bar{\sigma}$ and G are the elastic coefficient matrix, deviatric stress tensor, equivalent stress, and shear modulus constant, respectively. H' is the plastic tangent modulus. Using this constitutive equation, governing equations describing micro- and macroscopic deformation behavior are derived by homogenization theory.

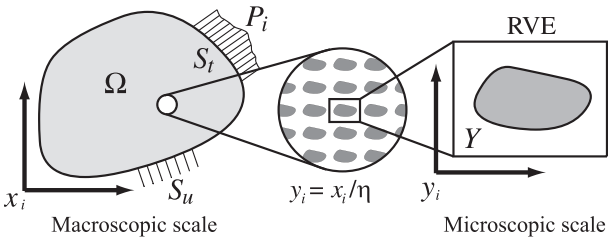

Fig. 1. Schematic illustration of two-scale boundary value problem.

We consider the two-scale boundary value problem for micro- and macroscopic scales as shown in **Fig. 1**. Here, x_i and y_i are macro- and microscopic coordinates, respectively. These scales are related to each other as $y_i = x_i/\eta$ with parameter η. Then, the principle of virtual work is defined as

$$\int_\Omega (\dot{S}_{ij} + \sigma_{mj} v_{i,m}) \delta v_{i,j} d\Omega = \int_{S_t} \dot{P}_i \delta v_i dS \,. \quad \ldots (8)$$

Boundary conditions for displacement rate vector v_i and traction force vector P_i are defined as

$$\begin{cases} \dot{P}_i = (\dot{S}_{ij} + \sigma_{mj} v_{i,m}) n_j & \text{on} \quad S_t \\ V_i = v_i & \text{on} \quad S_u \end{cases} . \quad (9)$$

where σ_{ij} and n_j are the Cauchy stress tensor and the normal vector on surface S_u, respectively. $\dot{S}_{ij}$ is the rate of the Kirchhoff stress tensor related to Eq. (7) as in the following equation:

$$\dot{S}_{ij} = \overset{\nabla}{S}_{ij} - F_{ijkl} \dot{\varepsilon}_{kl} \equiv L_{ijkl} \dot{\varepsilon}_{kl} \quad \ldots\ldots\ldots (10)$$

where F_{ijkl} is the total deformation gradient tensor.

In order to describe the deformation behavior of DP steel on micro- and macroscopic scales, we assume that the solution of the two-scale boundary value problem, v_i, is expressed as asymptotic expansion with respect to parameter η,

$$v_i(x_i, y_i) = \eta^0 v_i^0(x_i, y_i) + \eta^1 v_i^1(x_i, y_i) + \eta^2 v_i^2(x_i, y_i) + \cdots \quad \ldots\ldots\ldots\ldots\ldots\ldots (11)$$

where $v_i^j(x_i, y_i)$ stands for the j th order displacement rate vector. Introducing Eq. (11) into Eq. (8) and taking limit $\eta \to 0$, governing equations for micro- and macroscopic deformation behavior can be derived [13]. The governing equations for the macroscopic scale is given by the following equation:

$$\int_\Omega \left[L_{ijkl}^H \dot{E}_{kl}^0 + \tau_{ijkl}^H \frac{\partial v_k^0}{\partial x_l} \right] \frac{\partial \delta v_i}{\partial x_j} d\Omega = \int_{S_t} \dot{P}_i \delta v_i dS \quad . \quad (12)$$

Here, L_{ijkl}^H and τ_{ijkl}^H are the homogenized elastic constant and the homogenized material constant, respectively. These constants are given by the volume average of the

microscopic deformation property as follows:

$$L^H_{ijkl} = \frac{1}{|Y|}\int_Y \left\{ L_{ijkl} - L_{ijpq}\frac{1}{2}\left(\frac{\partial \chi^{kl}_p}{\partial y_q} + \frac{\partial \chi^{kl}_q}{\partial y_p} \right) \right\} dY \quad \ldots (13)$$

$$\tau^H_{ijkl} = \frac{1}{|Y|}\int_Y \left(\sigma_{lj}\delta_{ki} - \sigma_{mj}\frac{\partial \chi^{kl}_i}{\partial y_m} \right) dY \quad \ldots (14)$$

where χ^{kl}_p is the solution of the following governing equations for the microscopic scale and a periodic function in the microscopic scale, i.e., Y-periodic:

$$\int_Y \left\{ L_{ijpq}\frac{1}{2}\left(\frac{\partial \chi^{kl}_p}{\partial y_q} + \frac{\partial \chi^{kl}_q}{\partial y_p} \right) + \sigma_{qj}\delta_{pi}\frac{\partial \chi^{kl}_p}{\partial y_q} \right\} \frac{\partial \delta v_i}{\partial y_j} dY$$

$$= \int_Y \left(L_{ijkl} + \sigma_{lj}\delta_{ki} \right) \frac{\partial \delta v_i}{\partial y_j} dY \quad \ldots (15)$$

$\dot{E}^0_{kl}$ is the macroscopic strain tensor that is derived as a function of 0 th order displacement rate vector $v^0_i(x_i,y_i)$. Microscopic strain $\dot{\varepsilon}^0_{ij}$ and stress $\dot{S}^0_{ij}$ can be written as

$$\dot{\varepsilon}^0_{ij} = \dot{E}^0_{ij} - \frac{1}{2}\left(\frac{\partial \chi^{kl}_i}{\partial y_j} + \frac{\partial \chi^{kl}_j}{\partial y_i} \right) \dot{E}^0_{kl}, \quad \ldots (16)$$

$$\dot{S}^0_{ij} = L_{ijkl}\dot{\varepsilon}^0_{kl}, \quad \ldots (17)$$

In numerical simulation, we investigate micro- and macroscopic deformation behavior of DP steel by solving governing equations Eqs. (12) and (15) using the finite element method.

4. Simulation Procedure and Numerical Conditions

In this study, the two-dimensional MPF simulation of the $\gamma \to \alpha$ transformation in Fe-C-Mn alloy during CCT is performed in order to predict the morphology of the α phase in DP steel. Due to CCT, temperature continuously decreases from initial temperature $T_0 = 1100$ K at a constant cooling rate of 0.1 K/s. The size of the computational domain is 66×36 μm^2 and discretized by 165×90 regular meshes. The mesh size is 0.4 μm. The periodic boundary condition is used for the x and y directions. The initial configuration of the γ parent phase is produced by ordinary MPF simulation of grain growth. The number of initial γ grain is 17. Since triple-junction points of γ grain boundaries are preferable nucleation sites of α grains, we assume that all α grains are initially nucleated at triple-junction points. The number of initial α nuclei is 17 and its radius is assumed to be $r = 1.6$ μm. Initial carbon concentrations are in equilibrium for the α and γ phases. We assume that growth of the α phase does not depend on the crystal orientation of the α and γ phases. Material parameters and physical values are as follows [21]: $M_0 = 3.5 \times 10^{-7}$ m^4/(Js), $Q_0 = 140 \times 10^3$ J/mol, $D^\alpha_0 = 2.2 \times 10^{-4}$ m^2/s, $D^\gamma_0 = 1.5 \times 10^{-5}$ m^2/s, $Q_\alpha = 122.5 \times 10^3$ J/mol, $Q_\gamma = 142.1 \times 10^3$ J/mol, $\Delta S = 3.46 \times 10^5$ J/mol, $\gamma_{ij} = 0.5$ J/m^2 and $\delta = 2.8$ μm.

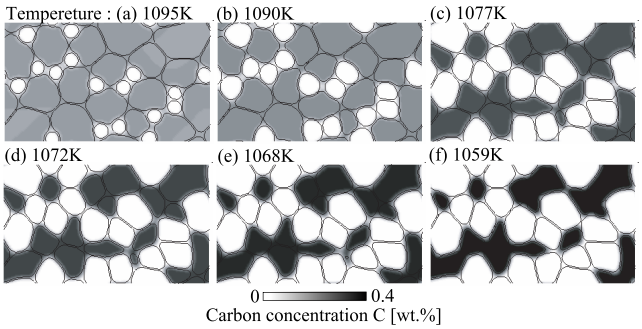

Fig. 2. Evolution of α grains and carbon concentration during $\gamma \to \alpha$ transformation.

After MPF simulation, we perform EP-FEA in order to investigate the deformation behavior of DP steel, including the α phase simulated during the tension-compression test. The configuration of the simulated α phase is modeled by the representative volume element (RVE). The geometry of the $\alpha + \alpha'$ DP microstructure is represented by a periodic array of RVEs. In this study, we assume that the untransformed γ phase after $\gamma \to \alpha$ transformation changes to the α' phase at room temperature and that the α' phase has a uniform structure. We generate the RVE and finite element mesh by using digital-image-based modeling, as explained in a previous paper [16].

EP-FEA of the tension-compression test of DP steel is conducted under uniform deformation for strain rate $\dot{E} = 10^{-3}$ /s. Because we simulate the two-dimensional morphology of the DP microstructure, the two-dimensional plane strain condition is assumed. The initial yield stress of α and α' phases is assumed to be 400 MPa and 1200 MPa, respectively. Young's modulus, Poisson's ration, and shear modulua are chosen as $E = 206$ GPa, $\nu = 0.3$, and $G = 80$ GPa, respectively.

5. Results and Discussion

5.1. Formation of the α Phase in $\gamma \to \alpha$ Transformation During Continuous Cooling Process

Figure 2 shows the simulated evolution of the α phase and the carbon concentration in $\gamma \to \alpha$ transformation during CCT. In this figure, the black solid line indicates a grain boundary. White and gray regions correnspond to α and γ phases, respectively. This result shows that α grains grow with carbon diffusion and carbon concentration in γ phase increases. Due to the increase in supersaturation in the γ phase, $\gamma \to \alpha$ transformation is suppressed as α grains grow. The variation in volume fraction of the α phase (V_f) is shown in **Fig. 3**. Although V_f increases monotonically from $T = 1100$ K, the transformation rate decreases with the decrease in temperature. From the above results, it is demonstrated that MPF sim-

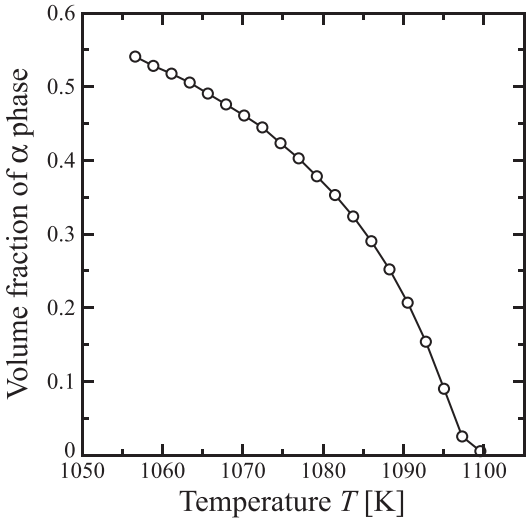

Fig. 3. Variation in the volume fraction of the α phase.

ulation allows us to understand microstructure evolution during $\gamma \rightarrow \alpha$ transformation. Furthermore, simulation results give us the distribution of the α phase at an arbitrary temperature and time. Therefore, using these simulated morphologies of the microstructure, we can investigate the mechanical properties of DP steel containing various V_f and morphologies of the α phase, as shown in the next section.

5.2. Deformation Behavior of DP Steel in the Tension-Compression Test

The tension-compression test of DP steel, including the simulated α phase, is performed using EP-FEA. Since we employ the homogenization method, the macro- and microscopic deformation behavior of the DP steel can be investigated simultaneously.

Figure 4 shows RVEs describing the α + α' DP microstructure. These RVEs represent a microstructure containing the α phase shown in **Figs. 2 (b)**, **(d)** and **(f)**, respectively. It is shown that the distribution of the simulated α phase is described in the RVE by using digital-image based modeling. For all RVEs, the total number of crossed-triangle elements and nodes are 4680 and 4838, respectively. The mesh size of a crossed-triangle element is $\Delta x = 0.53$ μm and $\Delta y = 0.90$ μm. V_f of the α phase in these RVEs are 29%, 56% and 67%, respectively. Therefore, DP steels whose microstructures are represented by RVEs are named DP-29% steel, DP-56% steel and DP-67% steel. We can find a difference in the microstructure of these DP steels. That is, the configuration of the α phase in DP-29% steel is isolated, while the connected configuration of the α phase is recognized in DP-56% and DP-67% steels. Using the above RVEs, EP-FEA of the tension-compression test of DP steel is performed and the effects of V_f and the configuration of α phase on deformation behavior and mechanical properties are investigated.

Figure 5 shows calculated macroscopic true stress-true strain curves of DP steel containing different DP microstructures (different RVEs). As we expect, strain hardening during tension deformation increases with the decreasing volume fraction of the soft α phase. Therefore, it is confirmed that the macroscopic deformation behavior of DP steel in initial tensile deformation is mainly governed by V_f of the α phase.

FEA based on the homogenization method allows us to study the relationship between the macroscopic stress-strain curve and deformation behavior inside the mi-

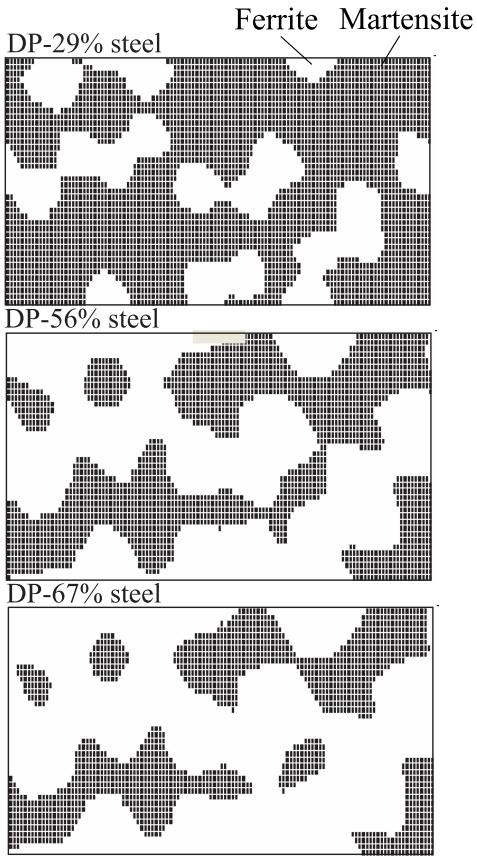

Fig. 4. RVEs describing the DP microstructure for different DP steels.

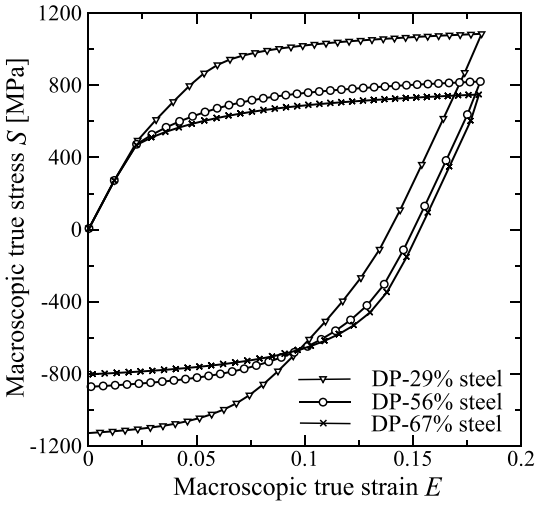

Fig. 5. Macroscopic true stress – true strain curves for different DP steels.

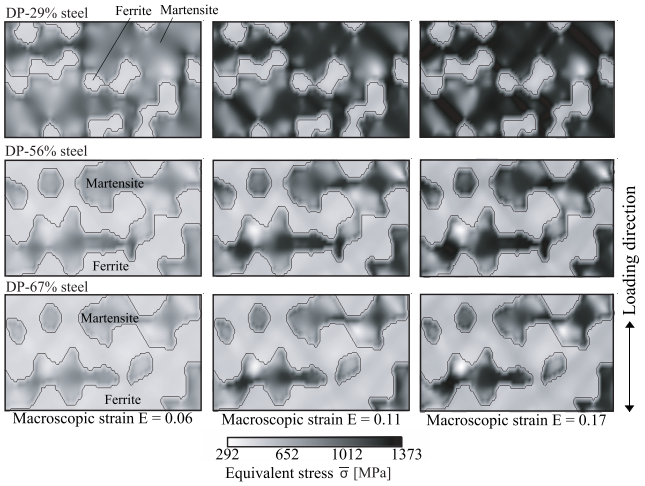

Fig. 6. Evolution of equivalent stress in the microstructure for different DP steels.

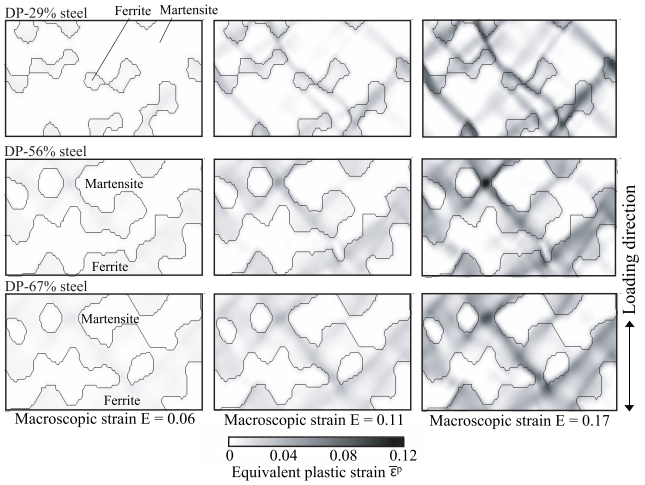

Fig. 7. Evolution of equivalent plastic strain in the microstructure for different DP steels.

crostructure. The evolution of equivalent stress in the microstructure during tension deformation for different DP steel is shown in **Fig. 6**. In all DP steel, it can be seen that the α' phase plays a role in the deformation resistance. Especially in the DP-29% steel, since each α grain is isolated and deforms little plastically, a high stress-field is exhibited in the α' phase. In DP-56% and DP-67% steel, because α grains are connected to each other, plastic deformation can easily occur in the α phase. As a result, we observed that stress concentration occurred only in the α' phase, which is located between the α grains.

Figure 7 shows the evolution of equivalent plastic strain in the microstructure in tension deformation for different DP steel. Plastic strain in the microstructure increases with increasing macroscopic strain. Distribution of plastic strain stongly depends on the configuration of the α phase. For all DP steel, when macroscopic strain reaches $E = 0.17$, it can be seen that plastic strain concentrates along the soft α phase and plastic deformation bands form in a direction at 45 degrees to the loading direction.

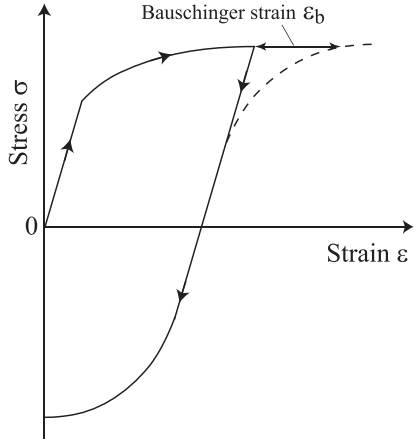

Fig. 8. Definition of Bauschinger strain.

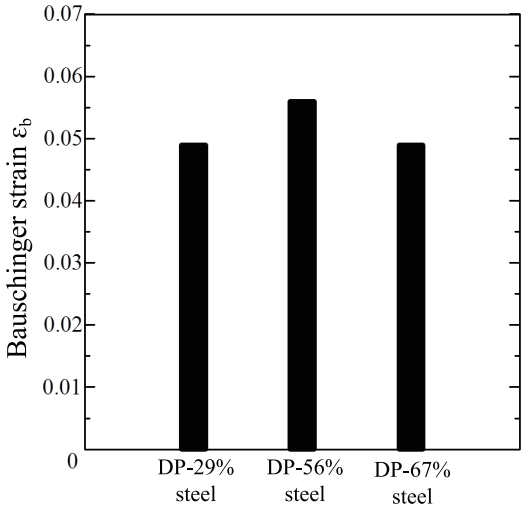

Fig. 9. Bauschinger strain for different DP steels.

Furthermore, as shown in **Fig. 5**, all DP steel exhibits the Bauschinger effect during the unloading and compression processes. The Bauschinger effect considered to be observed from the macroscopic stress-strain curve is influenced by inhomogeneous deformation in the microstructure. To evaluate the Bauschinger effect observed in this study, we calculate Bauschinger strain ε_b, which is defined as shown in **Fig. 8**, from macroscopic stress-strain curves shown in **Fig. 5**. ε_b calculated for all DP steel is shown in **Fig. 9**. It is found that DP-56% steel exhibits the largest ε_b in this study. To clarify the origin of the Bauschinger effect from the viewpoint of the microstructure, **Fig. 10** shows the evolution of equivalent plastic strain that is newly generated during the unloading and the compression processes. It was found that plastic strain develops significantlly in regions where small amounts of plastic strain is accumulated during initial tension deformation. In other words, the α phase in which large plastic strain is generated in tension deformation deforms plastically only negligibly during compression deformation due to strain hardening. We concluded that such inhomogeneous plastic deformation in the α phase during compression deformation causes the Bauschinger

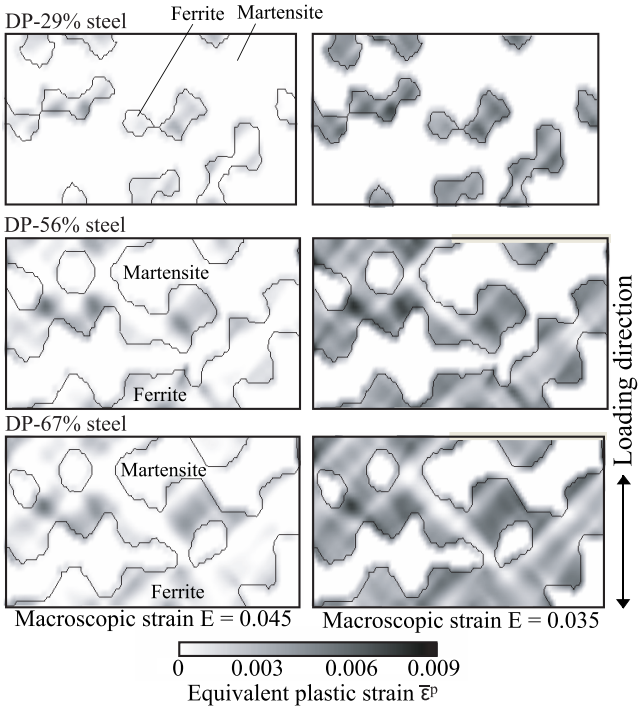

Fig. 10. Evolution of equivalent plastic strain in the microstructure during unloading and compression processes for different DP steels.

effect. The mechanism of the Bauschinger effect as explained above is similar to that reported previously in the literature [15].

6. Conclusions

In order to improve the mechanical properties of steel and to develop a novel high-strength steel, it is essential to predict the morphology of the microstructure in steel and its mechanical properties simultaneuously using numerical simulation. In this study, a coupled simulation method has been developed by using the MPFM and EP-FEA based on the homogenization method to predict the microstructure and mechanical properties of steel. We have applied the developed simulation method to investigating the formation of the α phase in a Fe-C-Mn alloy during CCT and deformation behavior of DP steel that is affected by the morphology of the α phase on micro- and macroscopic scales.

In the developed simulation method, with the help of the MPFM, we simulated the evolution of not only V_f of the α phase, but also of the morphological change in the microstructure during $\gamma \rightarrow \alpha$ transformation. Therefore, the simulated morphology of the α phase can be used for modeling the DP microstructure in DP steel. Using the RVE made by the morphology of the α phase predicted by MPF simulation, the effects of V_f and the configuration of the α phase on maco- and microscopic deformation behavior of DP steel have been clarified.

EP-FEA of the tension-compression test of DP steel including different DP microstructures has revealed that strain hardening during tension deformation increases with the decreasing V_f of the α phase. According to the result, we have confirmed that macroscopic deformation behavior of DP steel in initial tensile deformation is governed by V_f of the α phase. Furthermore, on the basis of microscopic investigation of deformation behavior in DP steel, we have clarified the mehanism of the Bauschinger effect depending on the microstructural morphology. That is, it has been found that the Bauschinger effect observed in compression deformation is governed by the plastic deformation behavior of the α phase, which does not deform plastically in initial tension deformation. Consequently, we have demonstrated that the author's simulation model enables us to systematically investigate macro- and microscopic deformation behavior of DP steel, including various V_f, and morphologies of the α phase.

Further improvement of the simulation method with the MPF and FEA based on the homogenization method as reported in this paper would allow us to more precisely predict the mechanical properties of steel on the basis of the microstrucuture. In order to improve the proposed simulation method in future work, introduction of crystal plasticity FEA is the most promising. The validation of the simulation result would be essential for the application of our simulation method to practical numerical simulation in material design and development.

Acknowledgements

This study was financially supported in part by ISIJ Research Promotion Grant from the Iron and Steel Institute of Japan and by Grant-in-Aid for Scientific Research for Young Scientists (B) of the Japan Society of the Promotion of Science (Project No. 23760088).

References:

[1] M. Calcagnotto, Y. Adachi, D. Ponge, and D. Raabe, "Deformation and fracture mechanisms in fine- and ultrafine-grained ferrite/martensite dual-phase steels and the effect of aging," Acta Materialia, Vol.59, pp. 658-670, 2011.
[2] T. Senuma, M. Suehiro, and H. Yada, "Mathematical Models for Predicting Microstructural Evolution and Mechanical Properties of Hot Strips," ISIJ Int., Vol.32, pp. 423-432, 1992.
[3] M. Suehiro, T. Senuma, H. Yada, and K. Sato, "Application of Mathematical Model for Predicting Microstructural Evolution to High Carbon Steels," ISIJ Int., Vol.32, pp. 433-439, 1992.
[4] N. Provatas and K. Elder, "Phase-Field Methods in Materials Science and Engineering," WILEY-VCH Verlag GmbH & Co. KGaA, Weinheim, Germany, 2010.
[5] I. Steinbach, F. Pezzolla, B. Nestler, M. Seeßelberg, R. Prieler, G. J. Schmitz, and J. L. L. Renzende, "A phase field concept for multiphase systems," Physica D, Vol.94, pp. 135-147, 1996.
[6] D. Fan and L.-Q. Chen, "Computer simulation of grain growth using a continuum field model," Acta Materialia, Vol.45, pp. 611-622, 1997.
[7] R. Kobayashi, "Modeling and numerical simulations of dendritic crystal growth," Physica D. Vol.63, pp. 410-423, 1993.
[8] J. A. Warren and W. J. Boettinger, "Prediction of dendritic growth and microsegregation patterns in a binary alloy using the phase-field method," Acta Metallurgica et Materialia, Vol.43, pp. 689-703, 1995.
[9] Y. Wang and A. G. Khachaturyan, "Three-dimensional field model and computer modeling of martensitic transformations," Acta Materialia, Vol.45, pp. 759-773, 1997.
[10] I. Loginova, J. Odqvist, G. Amberg, and J. Ågren, "The phase-field approach and solute drag modeling of the transition to massive $\gamma \rightarrow \alpha$ transformation in binary Fe-C alloys," Acta Materialia, Vol.51, pp. 1327-1339, 2003.
[11] T. Takaki, Y. Hisakuni, T. Hirouchi, A. Yamanaka, and Y. Tomita, "Multi-phase-field simulations for dynamic recrystallization," Computational Materials Science, Vol.45, pp. 881-888, 2009.

[12] T. Takaki, A. Yamanaka, Y. Higa, and Y. Tomita, "Phase-field Model during Static Recrystallization based on Crystal-plasticity Theory," J. of Computer-aided Materials Design, Vol.14, pp. 75-84, 2007.
[13] J. M. Guedes and N. Kikuchi, "Preprocessing and postprocessing for materials based on the homogenization method with adaptive finite element methods," Computer Methods in Applied Mechanics and Engineering, Vol.83, pp. 143-198, 1990.
[14] K. Terada and N. Kikuchi, "A class of general algorithms for multi-scale analyses of heterogeneous media," Computer Methods in Applied Mechanics and Engineering, Vol.190, pp. 5427-5464, 2001.
[15] K. Terada, K. Matsui, M. Akiyama, and T. Kuboki, "Numerical re-examination of the micro-scale mechanism of the Bauschinger effect in carbon steels," Computational Materials Sciences, Vol.31, pp. 67-83, 2004.
[16] A. Yamanaka, T. Takaki, and Y. Tomita, "Coupled simulation of microstructural formation and deformation behavior of ferrite-pearlite steel by phase-field method and homogenization method," Materials Science and Engineering. A, Vol.349, pp. 244-252, 2008.
[17] I. Steinbach and F. Pezzolla, "A generalized field method for multiphase transformations using interface fields," Physica D, Vol.134, pp. 385-393, 1999.
[18] J. Eiken, B. Böttger, and I. Steinbach, "Multiphase-field approach for multicomponent alloys with extrapolation scheme for numerical application," Physical Review E, Vol.73, p. 066122, 2006.
[19] J. Tiaden, B. Nestler, H. J. Diepers, and I. Steinbach, "The multiphase-field model with an integrated concept for modelling solute diffusion," Physica D, Vol.115, pp. 73-86, 1998.
[20] M. Militzer, M. G. Mecozzi, J. Sietsma, and S. van der Zwaag, "Three-dimensional phase field modelling of the austenite-to-ferrite transformation," Acta Materialia, Vol.54, pp. 3961-3972, 2006.
[21] A. Yamanaka, T. Takaki, and Y. Tomita, "Simulation of Austenite-to-ferrite Transformation in Deformed Austenite by Crystal Plasticity Finite Element Method and Multi-phase-field Method," ISIJ Int., Vol.52, pp. 659-668, 2012.
[22] Y. Tomita, "Numerical Elasto-Plastic Mechanics," Yokendo Ltd, 1990. (in Japanese)
[23] S. J. Hollister and B. A. Riemer, "Digital image based finite element analysis for bone microstructure using conjugate gradient and Gausian filter technique," Mathematical Methods in Medical Imaging II, Vol.2035, pp. 95-106, 1993.

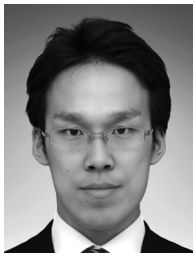

Name:
Akinori Yamanaka

Affiliation:
Associate Professor, Graduate School of Engineering, Tokyo University of Agriculture and Technology

Address:
2-24-16 Nakacho, Koganei, Tokyo 184-8588, Japan

Brief Biographical History:
2001-2005 Faculty of Engineering, Kobe University
2005-2008 Graduate School of Science and Technology, Kobe University
2008-2012 Assistant Professor, Graduate School of Science and Engineering, Tokyo Institute of Technology
2012- Associate Professor, Graduate School of Engineering, Tokyo University of Agriculture and Technology

Main Works:
• A. Yamanaka, T. Takaki, and Y. Tomita, "Simulation of Austenite-to-ferrite Transformation in Deformed Austenite by Crystal Plasticity Finite Element Method and Multi-phase-field Method," ISIJ Int., Vol.52, pp. 659-668, 2012.
• A. Yamanaka, T. Aoki, S. Ogawa, and T. Takaki, "GPU-accelerated phase-field simulation of dendritic solidification in a binary alloy," J. of Crystal Growth, Vol.318, pp. 40-45, 2011.

Membership in Academic Societies:
• The Japan Society of Mechanical Engineers (JSME)
• The Iron and Steel Institute of Japan (ISIJ)
• The Society of Materials Science, Japan (JSMS)
• The Japan Society for Technology of Plasticity (JSTP)
• The Japan Society for Computational Engineering and Science (JSCES)

Name:
Tomohiro Takaki

Affiliation:
Associate Professor, Graduate School of Science and Technology, Kyoto Institute of Technology

Address:
Goshokaidoucho, Matsugasaki, Sakyo, Kyoto 606-8585, Japan

Brief Biographical History:
1991-1995 Faculty of Mercantile Marine Science, Kobe University of Mercantile Marine
1995-1997 Graduate School of Maritime Science and Technology, Kobe University of Mercantile Marine
1997-2003 Assistant Professor, Faculty of Mercantile Marine Science, Kobe University of Mercantile Marine
2003-2007 Assistant Professor, Graduate School of Maritime Sciences, Kobe University
2007- Associate Professor, Graduate School of Science and Technology, Kyoto Institute of Technology

Main Works:
• T. Takaki and H. Kashima, "Numerical Investigations of Stress in Dendrites Caused by Gravity," J. of Crystal Growth, Vol.337, pp. 97-101, 2011.
• T. Takaki, A. Yamanaka, and Y. Tomita, "Multi-phase-field Simulations of Dynamic Recrystallization during Transient Deformation," ISIJ Int., Vol.51, pp. 1717-1723, 2011.

Membership in Academic Societies:
• The Japan Society of Mechanical Engineers (JSME)
• American Society of Mechanical Engineers (ASME)
• The Iron and Steel Institute of Japan (ISIJ)
• The Society of Materials Science, Japan (JSMS)
• The Japan Institute of Metals (JIM)
• The Japan Institute of Light Metals (JILM)
• High Pressure Institute of Japan (HPIJ)
• The Japan Society for Computational Engineering and Science (JSCES)